Journal of Applied Fluid Mechanics, Vol. 16, No. 3, pp. 491-504, 2023.
Available online at www.jafmonline.net, ISSN 1735-3572, EISSN 1735-3645.
https://doi.org/10.47176/jafm.16.03.1351

Analysis of Blood Flow Bifurcation Phenomena in Mitral Valve: A Numerical Approach to Predict Cardiac Arrest

S. Saha[1†], P. Biswas[2], A. N. Das[3], A. Kumar[1] and M. Kumar Singh[1]

[1] *Division of Mathematics, School of Advanced Sciences, Vellore Institute of Technology Chennai, Tamilnadu-600127, India*
[2] *Department of Mathematics, National Institute of Technology Silchar, Silchar-788010, Assam, India*
[3] *Department of Mathematics, Alipurduar University, Alipurduar, West Bengal-736121, India*

†*Corresponding Author Email: sandip.saha@vits.ac.in*

(Received June 6, 2022; accepted October 22, 2022)

ABSTRACT

Employing FVM, we have investigated numerically the rheological behavior of bifurcation phenomena of blood flow at various Reynolds numbers (Re) and at various values of contraction ratio (h), defined as the ratio of the inlet to narrow sections width of a two-dimensional planner contraction-expansion channel. Blood flow bifurcation through a planar contraction-expansion channel is analogous to the case of regurgitation (i.e., abnormal leakage of blood) in the mitral valve. In this work, we have studied the blood flow bifurcation characteristics including the normalized axial velocity profile, velocity gradient, dimensionless pressure, dimensionless longitudinal pressure gradient, pressure and skin friction coefficients on both the channel walls and analyzed the pressure drop, excess pressure drop for different values of *Re*. Secondly, blockage in the mitral valve is studied for different values of h. Pressure drops for various values of h are also studied to measure blood pressure. Correlation analyses are presented for normalized vortex length in terms of critical values of *Re* and h. It is revealed that if *Re* goes on increasing to 14.4 or more, flow breaks the symmetry at h = 15, and for each h, recirculation length increases linearly with the increase in *Re* but decreases valve flaps that reduce blood flow to the heart muscles.

Keywords: Contraction-expansion channel; Pressure drop; Pressure recovery factor; Bifurcation; Streamline; Numerical simulation.

1. INTRODUCTION

Through a leaking mitral valve, blood flow takes place in two ways. Firstly, due to contraction of the left ventricle, some amount of blood flows through the aorta from the ventricle, and then the rest of that returns to the atrium, which may cause cardiac arrest (Zhao *et al.* 2013). The phenomena of bifurcated blood flow in a sudden contraction-expansion channel have wide pragmatic applications in fluid mechanics; and that in the planer contraction channel causes many cardiovascular diseases. The proficiency of such channels is based on the channel contraction ratio, h. Bifurcation of flow (Chedron *et al.* 1978) arises in electronic cooling equipment, blending vessels, etc. (Shamloo *et al.* 2016; Shamloo and Parast 2019; Boodaghi and Shamloo 2020; Verlinden *et al.* 2020; Ashkezari *et al.* 2022), and it occurs in the case of blood flow in mitral valve because of the irregular spillage of blood, (Fig. 2). For the first time, Abbot and Kline (1962) solved numerically the problems considering plane sudden expansion (Fig. 1a). Experimental studies have been done on the subsonic turbulent flow for single and double backward-facing steps (Hajji *et al.* 2021). They observed that three distinct flow separations exist, viz., i) two-dimensional flow separation, ii) three-dimensional flow separation, and iii) overall separation of length. Severe effects of the *Re* and turbulence intensities on both the flow patterns and reattachment length have been discussed in their work. Sobey and Drazin (1986) analyzed a two-dimensional laminar flow in an indented channel (Fig. 1b) using analytical, numerical, and experimental methods. At a large value of *Re*, the time-periodic asymmetric flow was observed, whereas symmetric flow was noted for small values of *Re*. Their work also indicates the presence of a supercritical pitchfork bifurcation, and stable asymmetric flow if *Re* becomes too large. Shapira *et al.* (1990) studied the instability of symmetric, two-dimensional viscous flows with semi-angle (γ), $10^0 \leq \gamma \leq 90^0$, and *Re* based on a small expansion ratio in a symmetric expansion channel (Fig. 1d). To study the stability limit, linear stability analysis has been

employed for the half-domain and a minimum value of *Re* (Re_{cr}) has been detected. It is observed that for $Re \geq Re_{cr}$, flow changes from symmetric to asymmetric. Using experimental and numerical methods, Fearn *et al.* (1990) analyzed how steady asymmetric flow arises in a sudden symmetric expansion channel and revealed that the flow becomes time-dependent at the large value of *Re*.

Durst *et al.* (1993) provided a detailed study of velocity and predicted numerically that for *Re*>125 flow symmetry in the walls of a two-dimensional duct having an expansion ratio of 1:2 is lost. They also observed that if *Re*>125, the upper corner vortex length remains almost the same. Chen *et al.* (1995) numerically studied the flow bifurcation past a cylinder (Fig. 1c) kept within a couple of parallel planes. They studied symmetry-breaking bifurcation and Hopf bifurcation, and concluded that if $Re>Re_{cr}$, the flow region loses its stability. Numerical simulations of their work revealed that the existence of steady flow perturbation, time-dependent motion, and the flow perturbation dies at small values of *Re* for blockage ratio = 0.2. It is also shown that the

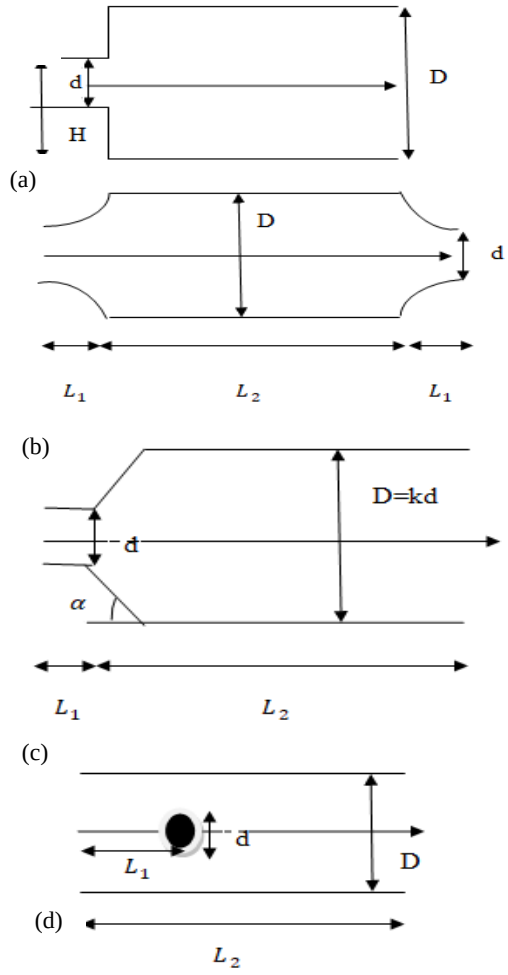

Fig. 1. Different types of flow geometries: (a) sudden expansion channel, (b) intended channel, (c) a cylinder between two parallel planes, (d) gradually expanded channel (Chedron *et al.* 1978).

perturbation increases as *Re* increases beyond its critical value, and evidently, the flow settles for a new state that generates time-periodic motion.

Balloch *et al.* (1995) considered incompressible Newtonian fluid flow in two and three-dimensional channels for very small values of *Re* only. To find the steady-state solutions, they employed time-stepping techniques for small and large values of expansion ratios. Numerical simulations asserted the existence of lip vortices (*Re* = 2.5) and salient vortices (*Re*> 10) at the corners, which has a strong agreement with their experimental results. The flow fields in a two-dimensional channel were numerically studied by Battaglia *et al.* (1997) to understand the occurrence of symmetric and asymmetric flows with the change in expansion ratio. Their results show that the variation in expansion ratio and critical *Re* are of opposite characteristics (Drikakis 1997). Touzopoulos and Bergeles (1998) showed that the laminar flow in a plane sudden expansion channel becomes symmetric when $Re \geq Re_{cr}$. Astarita and Greco (1968) calculated the excess pressure drop for contraction geometry experimentally and analytically and showed that the correlation between the Hagenbach and Couette corrections for pressure is lost. Ghosh *et al.* (2012) depicted flow patterns of different forms of core annular flow for high and low viscous oil-water emulsion through a sudden contraction and expansion channel. They also studied various types of interfacial distributions in the kerosene-water systems. In addition to that, the flow of lube oil-water has also been analyzed. It is observed that the pressure profiles and pressure loss coefficients are independent of the viscosity of the liquid and flow patterns for both lube oil-water and low viscous oil-water flows. Saha *et al.* (2020); Saha (2021a, b); Saha *et al.* (2022) solved a few problems on flow phenomena in a horizontal expansion channel.

Patlazhan *et al.* (2017) have studied the characteristics of bifurcated Newtonian-fluid flow in a two-dimensional sudden contraction-expansion channel and observed that if $Re>Re_{cr}$ length of the lower corner vortex increases faster than that of the upper corner vortex. Moreover, if *Re* increases further new vortexes are generated, which characterizes that the flow is driven by pressure, (Boughamoura *et al.* 2003). Mishra and Jayaraman (2002) solved the problem of symmetry-breaking flow of the generalized Newtonian fluid through a sudden planner expansion (Saha *et al.* 2021; Saha and Das 2022). Asymmetry in Geometry is observed on a small scale for small values of *Re*. Moreover, when $Re \leq Re_{cr}$ two successive similar flow transitions are found. For laminar Newtonian flow, many authors (Tsai *et al.* 2007; Ternik 2010; Dhinakaran *et al.* 2013; Moallemi and Brinkerhoff 2016) have determined the critical value of *Re* for various expansion ratios. Several authors have investigated the effect of expansion ratio (Oliveira *et al.* 2008; Saha and Das 2021) on non-Newtonian fluid flow. Pal and Hwang (1997) and Sanmigue *et al.* (2010) have also studied the nature of fluid flow through a two-dimensional

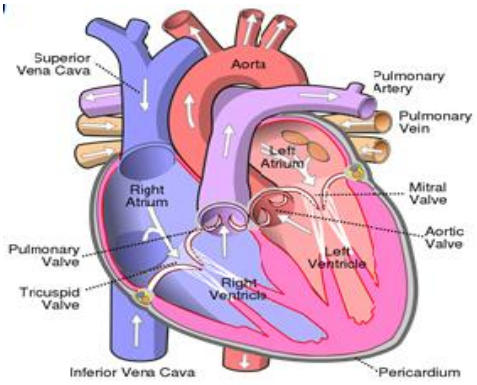

(a)

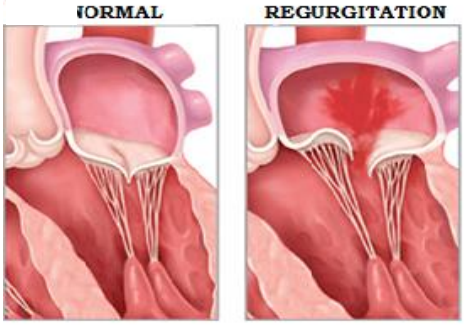

(b)

Fig. 2. (a) Location of Mitral Valve (https://myheart.net/articles/mitral-regurgitation/), and (b) Blood leakage in mitral valve (https://en.wikipedia.org/wiki/Mitral_valve).

sudden contraction channel. The cardiovascular framework supplies oxygenated blood to the tissues and organs of the human body. It consists of three parts, viz., heart, pulmonary circulations, and microvasculature. The oxygenated blood through the living tissues (Wang and Parker 2004; Korakianitis and Shi 2006; Formaggia *et al.* 2009) is supplied to the left heart and non-oxygenated blood returns to the right heart through veins. In pulmonary circulation, non-oxygenated blood is catapulted by the right heart streams through the aspirator routes towards the lungs. After being oxygenated there, it returns to the left heart through the pulmonary veins, as shown in Fig. 2. The blood pressure wave propagation, and models of blood flow are discussed in the references (Bakirtas and Demiray 2005; Davies *et al.* 2006), which give a clear idea of the blood flow models.

Here, we have considered the sudden contraction-expansion channel like the geometric features of mitral regurgitation. SIMPLEC algorithm (Van Doormaal and Raithby 1984) is applied for solving the governing equations, while the numerical simulations are performed using fluent software. The study includes the determination of Re_{cr}, needed for symmetry-breaking bifurcation at h = 15, and observation of the asymmetric flow patterns, which arise after a certain value of *Re*. The effect of different values of h $(4 \leq h \leq 15)$ is also investigated at *Re* = 29. Moreover, eight basic characteristics including the normalized axial velocity profile, normalized axial velocity gradient,

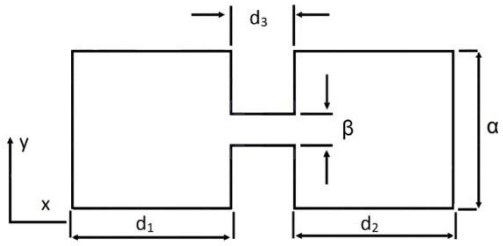

Fig. 3. Schematic diagram of sudden contraction-expansion channel: $d_1 = 0.15\ m$, $d_2 = 0.45\ m, d_3 = 0.01\ m$, $\beta = 0.002\ m, \alpha = 0.03\ m$.

dimensionless pressure, dimensionless longitudinal pressure gradient, pressure coefficients, skin friction coefficients on both lower and upper walls, kinetic energy, as well as the pressure drop are also calculated to investigate the flow bifurcation phenomenon. Furthermore, variation in pressure drop is plotted for the above set of values of h to examine the blood pressure categories.

2. PHYSICAL DOMAIN

In this work, we have considered 2-D viscous laminar flow to study the behavior of blood flow through a mitral valve, as shown in Fig. 3. The domain of interest is made of the inlet and outlet sections of equal width α, and a thin section of width β, h = $\frac{\alpha}{\beta}$, is defined as the contraction ratio.

3. PROBLEM FORMULATION AND NUMERICAL METHODS

Here, fluid flow is considered two-dimensional laminar, unsteady, Newtonian, and viscous. In this analysis, momentum and continuity equations are considered as follows:

$$\frac{\partial U}{\partial t} + (U.\nabla)U = -\frac{1}{\rho}\nabla P + \eta\nabla^2 U \quad (1)$$

$$\nabla.U = 0 \quad (2)$$

, where ρ, and η denote density and kinematic viscosity respectively. Here, U(x, t) and P(x, t) are defined as velocity vector and pressure. Blood is taken as Newtonian fluid in the present analysis with $\rho = 1.06 \times 10^3$ kg/m^3, μ (dynamic viscosity)= 0.005 Pa-s.

The Boundary conditions of the proposed problems are as follows:

• Inflow velocity, $U_{in} = U_0$ (Table 1).

• In the outlet section, we have assumed $\frac{\partial U}{\partial x} = 0$.

• At the boundary walls, we have prescribed $\frac{\partial U}{\partial x} = 0$ (no slip occurs), and $\frac{\partial U}{\partial y} = 0$ (no penetration occurs).

SIMPLEC algorithm is employed to solve equations 1 and 2, and the convergence criteria of the simulation are considered as $\|U_{n+1} - U_n\| \leq \epsilon$ and

Table 1 Inflow velocity for different Re

Re	U_0	*Re*	U_0
0.1	0.000235849	29	0.068396226
0.9	0.002122642	32	0.075471698
12	0.028301887	39	0.091981132
14	0.033018868	42	0.099056604
14.4	0.033962264	52	0.122641509
23	0.054245283	62	0.146226415
72	0.169811321	120	0.283018868
82	0.193396226	145	0.341981132
92	0.216981132	160	0.377358491
98	0.231132075	180	0.424528302

$\|P_{n+1} - P_n\| \leq \epsilon$ with $\epsilon = 10^{-6}$. Dimensionless variables are defined as:

$U^* = U\beta/\eta$, $x^* = x/\beta$, $P^* = P\rho\beta^2/\mu^2$, $L_v = l_v/\alpha$ (where v = 1, 2, 3, 4), *Re*= $U_{max}\beta/\eta$, where U_{max} denotes the maximum velocity.

3.1. Numerical Procedures

Ansys Fluent has been used for simulation and visualization purposes. Variables defined at the center of the control volume populating the physical domain have been considered for solving the governing equations using FVM. Integration of each equation over each control volume provides a discrete equation that links the variable at the center of the volume to its neighbors. Despite some compelling features of FVM, the lower-order interpolation of the convective terms in the governing equations causes several unwanted numerical effects. To avoid those, the QUICK scheme (Leonard 1979) has been utilized for spatial discretization of convective terms in the momentum equation. It is a differencing system in computational fluid dynamics that considers a three-point upstream weighted quadratic interpolation for the cell face values. For the phenomena of flow characteristics, the Quick-scheme is used for the interpolations, and a second-order upwind scheme is applied for the pressure terms. Moreover, it is a three-point technique, which is third-order accurate on uniform meshes and is based on quadratic polynomial interpolation. It is an upwind scheme, and accurate up to the 3rd order for the advection terms, but the 2nd order for the rest of the terms (diffusion terms). SIMPLEC algorithm (Van Doormaal and Raithby 1984; Ternik *et al.* 2006) resolves the coupling between velocity and pressure. As a result, using the SIMPLEC technique (Van Doormaal and Raithby 1984; Ternik *et al.* 2006), updated velocity and pressure field satisfying exactly mass balance and essentially discrete momentum equations have been found. The convergence measure is set as 10^{-6}, and 10^{-6} for the considered equations.

3.2. Mesh Study

A qualitative solution at low computational cost can be found through mesh study. The Meshing of the whole domain has been divided into three different zones with three types of uniform rectangular meshes for inlet, narrow, and outlet sections as shown in Fig. 4. Taking *Re* = 23 and h = 15, flow

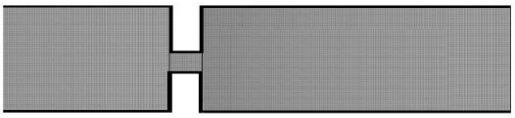

Fig. 4. Mesh geometry at h = 15.

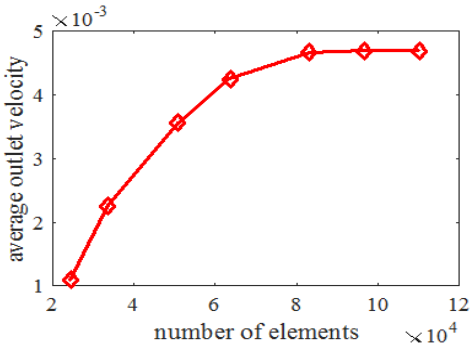

Fig. 5. Number of elements vs. average outlet velocity at *Re* = 23, h = 15.

bifurcation is analyzed with the aid of a pressure-based solver. Figure 5 depicts that for efficient and quantitative simulation the optimum number of cells is 82,942.

3.3. Validation

The Numerical results of this work have been validated with those of Patlazhan *et al.* (2017), and have been depicted in Fig. 6 (a-b). For the same input parameters, Fig. 6(a) and Table 2(a-b) show the closeness of the outcomes of this work with those of Patlazhan *et al.* (2017).

The bifurcation diagram is presented in the x-y plane with *Re* along the x-axis and normalized vortex length along the y-axis. Figure 6(a) depicts that for both the corner vortices, the bifurcation length remains the same for a certain value of *Re* (Re_{cr}). However, when $Re > Re_{cr}$ both the corner vortices break the symmetry. It can be seen that bifurcation starts at a particular time (Fig. 6b). In Table 2, the percentage error is calculated as, % error= | [(Patlazhan *et al.* 2017)-present study)/Patlazhan *et al.* (2017)] | ×100%.

Table 2 (a-b) % error of Patlazhan *et al.* (2017) vs. present work.

a. lower corner vortex length, L_1			b. upper corner vortex length, L_2		
Re	Patlazhan et al. (2017)	Present study	*Re*	Patlazhan et al. (2017)	Present study
0.779	0.217	0.2159	0.779	0.217	0.2159
16.5	1.01	0.99	16.5	1.01	0.99
25.6	2.04	2.03	25.6	0.873	0.863
30.8	2.24	2.22	30.8	0.885	0.8825
total percentage error= 0.25			total percentage error= 0.25		

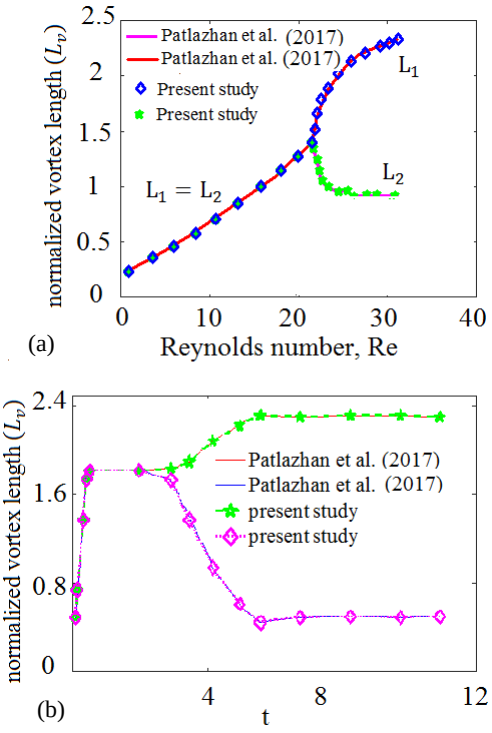

Fig. 6. (a) Bifurcation diagram at various *Re*, (b) normalized vortex length vs. different time at $Re = 28.6$.

4. RESULTS AND DISCUSSIONS

For different values of *Re*, the separation and reattachment of corner vortices have been discussed in this sub-section.

4.1. Flow Structure and Recirculation Characteristics at Various *Re*

It is shown that three different types of flow configuration, viz., creeping flow, symmetric jet, and asymmetric jets evolve with the increase in *Re*. For small values of *Re*, creeping flow arises and the flow becomes symmetric for sufficiently large values of *Re*, and due to further increase in *Re* the flow losses its' symmetry. The streamlines for the contraction ratio, and various values of *Re* from 0.1 to 42, have been presented in Fig. 7. It is clear that for creeping flow (Fig. 7(a-b)), bifurcation occurs on a small scale at the corner of both the walls for *Re*< 10, but if the value of *Re* crosses 10, two vortices of the same length occur at the corner walls of the channel as shown in the Fig. 7(a-c). Moreover, if *Re* goes on increasing to 14.4 or more, the flow breaks the symmetry as shown in Fig. 8(d). It is observed that the number of vortices increases as *Re* increases. In Fig. 7(e-g), it is depicted that the flow becomes asymmetric with the increase in *Re*, and as a result, circulation becomes more complex, which causes a decrease in blood flow in the valve.

4.2. Bifurcation Diagram for Different *Re* at h= 15

Figure 8 presents the bifurcation diagram, which

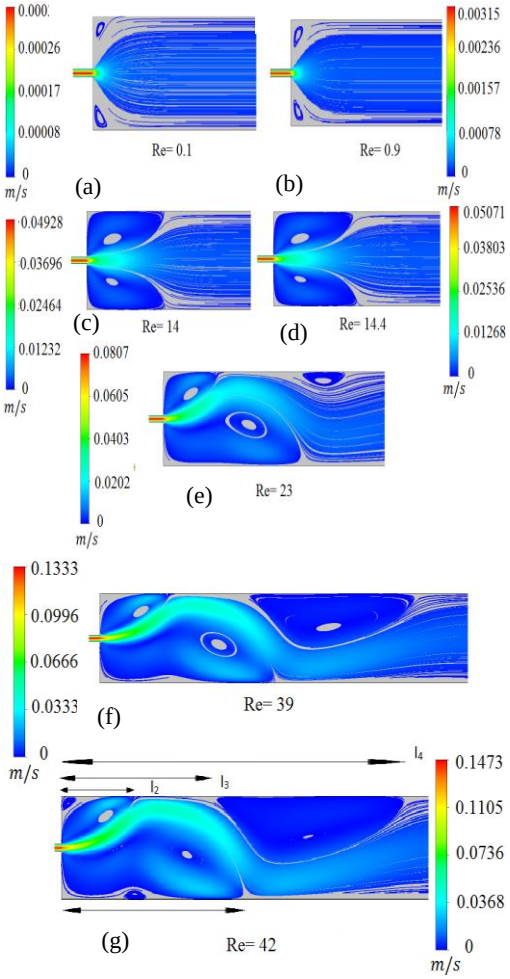

Fig.7 (a-g). Streamlines of blood flow at various *Re*.

depicts normalized vortex lengths at different values of *Re* at the corner walls of the channel. From Fig. 7 and 8, it is clear that at $Re = 0.1$, the first bifurcation of the flow occurs at both the corner walls, and for $Re < 14.4$, the flow patterns remain symmetric (i.e., the vortices remain of uniform sizes). It is also found that for the values of *Re* satisfying $0.1 \leq Re \leq 14.39$, corner vortices are developed consistently and linearly ($L_1 \approx L_2$). But, for $Re \geq 14.4$ one corner vortex increases in size, while that of the other corner vortex starts to reduce showing that the symmetry of the flow changes to a stable one (Fig. 7(d-g), 8). With the increase in *Re*, more than two separate zones arise at the corner walls of the channel as shown in Fig. 7(e-g) and 8. Similar flow patterns occur for different contraction ratios and different widths of the narrow section, as shown in Fig. 8.

4.3. Effects of h

For different values of $h \in [4, 13.5]$, and a fixed value of $Re\ (= 29)$, details of the flow patterns are discussed in this subsection, and the downstream of the sudden contraction expansion channel, flow bifurcation phenomena are presented. Figure 10 depicts that for the values of $h \in [10, 13.5]$, the

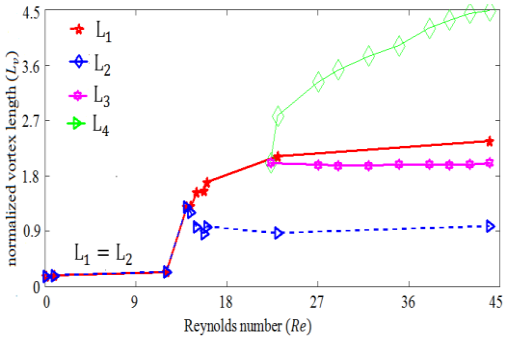

Fig. 8. Effect of *Re*.

flow symmetry is lost. It is also studied that the length of the recirculation zones increases as the channel depth increases from 4 to 13.5. Consequently, the strength of the secondary flow reduces and gives a stable flow pattern in the corner walls, preventing asymmetries from the start of the flow. From Fig. 9(a, b), it is evident that for h = 4,5, the flow remains symmetrical with its length equal to vortex lengths (L_1 = L_2) nearly, and the flow symmetry disappears as the value of contraction ratio increases. However, at h = 7.5, it is found that two different corner vortices appear (Fig. 10(c)), but for h ≥ 10 more than two corner vortices exist at the corner walls of the channel (Fig. 10(d-f)]. Figures (10-11) depict various normalized vortex lengths with different values of *Re* and contraction ratios. From these figures, it is clear that for $Re < Re_{cr}$, flow breaks the symmetry and the vortices at the upper corner wall are shrinking, but those in the lower corner wall grow sharply. For this, the flow changes from symmetric to asymmetric due to small disturbances. Equation 3 represents a function of Re for various contraction ratios, h ∈ [4, 15], which is fitted to generate a linear relationship between normalized vortex length and *Re*. It is found that an increase in *Re* increases recirculation length for each h (Fig. (10-11)).

$$L_v = 0.1471 + 0.00421h - 0.00035Re - 0.00021\,Re\,h + 0.001Re\sqrt{h} \quad (3)$$

For a sufficiently large value of Re, the flow becomes asymmetric with the increase in contraction ratio, and the correlation function generates an inverse relationship between Re_{cr} and h (Fig. 12). The flow bifurcation was computed at $Re < Re_{cr}$ until a steady state mode is achieved. The sudden expansion can amplify the small disturbance existing in the incoming laminar flow (Castillo *et al.* 2014).

$$Re_{cr} = \frac{50.63}{e^{0.0916h}} \quad (4)$$

Thus, Re_{cr} has been noted as the minimum value of *Re* at which the bifurcation occurs, as shown in Fig. 12. The square of the regression coefficient (R^2) is found to be equal to 0.7265 for the contraction ratio, h = 4, 5, and 7.5, while the same is equal to

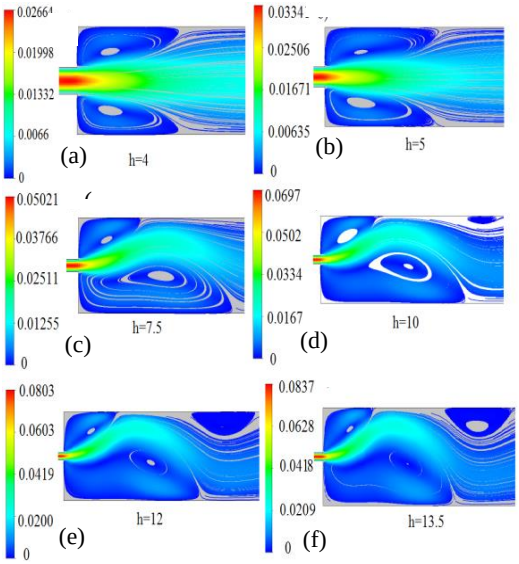

Fig. 9. Streamlines for different h at *Re* = 29.

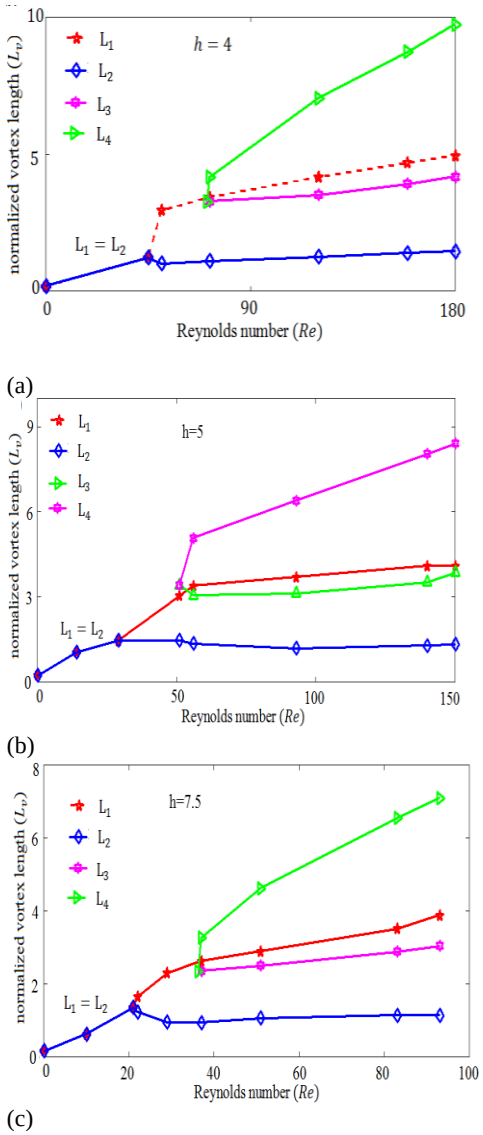

Fig. 10. Bifurcation diagram for various *Re* at (a) h = 4, (b) h= 5 and (c) h= 7.5.

0.9965 for h = 12, 13.5, and 15. Thus, an increase in f causes an increase in the regression coefficient. Moreover, from the Fig. (10-12) it is found that 45.4 is the critical value of *Re* at h = 4, while Re_{cr} is equal to 28.9 at h = 5. However, for h = 7.5, 10, 12.5 and 13.5, the values of Re_{cr} are 21.4, 17.9, 16.2, and 15.2 respectively. Furthermore, normalized vortex length increases with the decrease in contraction ratio as can be seen in the Fig. (10-11). For different values of contraction ratio, Fig. 13 shows the variation in asymmetry parameter with *Re*. Here A_s is defined as, $A_s = 2L_s - (L_1 + L_2)$, where L_s denotes the larger value of vortex length. Moreover, it is seen that at a particular value of h, the asymmetry parameter linearly increases with the increase in *Re* (Fig. 10(a-c) and 11(a-c)).

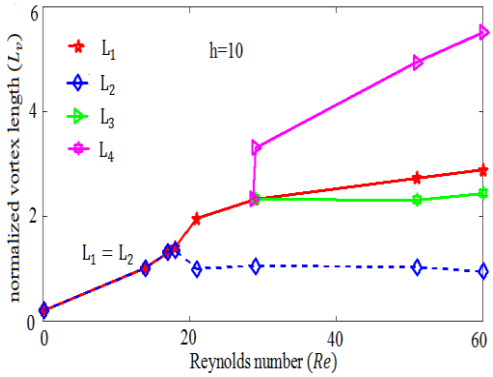

(a)

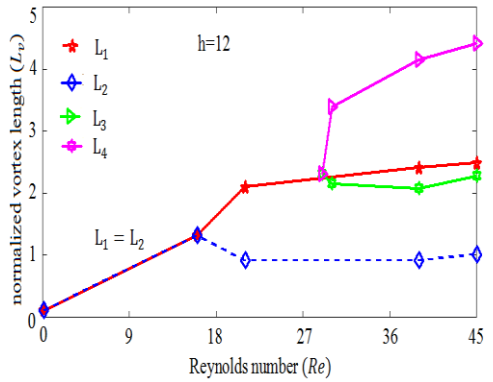

(b)

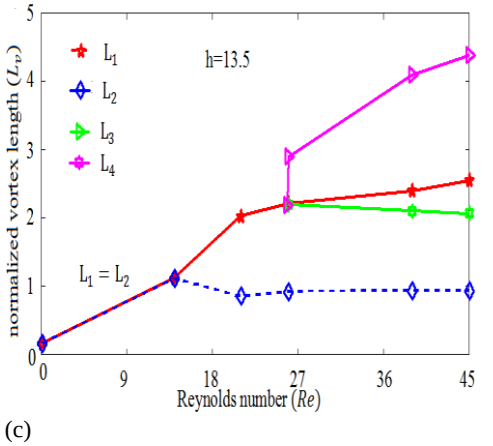

(c)

Fig. 11. Bifurcation diagram for various *Re* at (a) h = 10, (b) h= 12 and (c) h= 13.5.

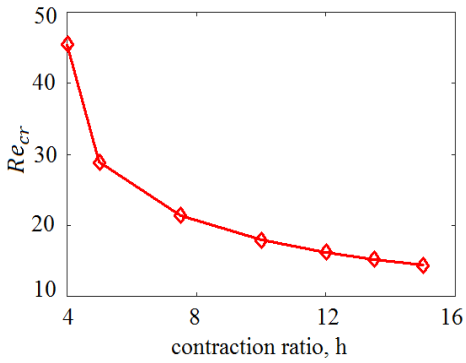

Fig. 12. Plots of h vs Re_{cr}.

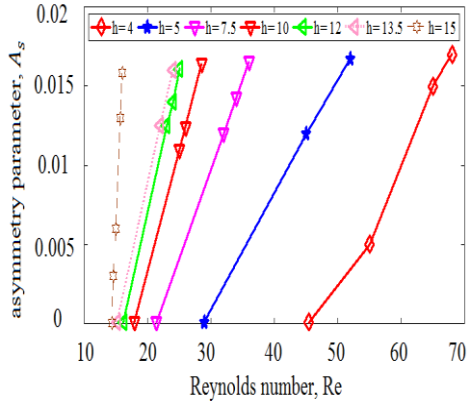

Fig. 13. Variation of asymmetry parameter with *Re* at various h.

4.4. Velocity and Pressure Profile at h = 15

Figures 15(a-b), 16 and 17(a-b) depict the sudden variation in the velocity and pressure due to the change in the channel width. Consequently, the axial velocity is increased unusually and causes a pressure drop. The mechanism of bifurcation is based on the propagation of velocity disturbance, which depends on *Re*. In Fig. 7, 9, and 15, it is shown that velocity increases in the region close to the channel walls. It is seen that centerline velocity decreases when the fluid moves downstream of the channel. The variations in the horizontal component of axial velocity and longitudinal velocity gradient for various *Re* are presented in Fig. 15(a-b) and 16. Variations in the velocity are mainly observed in the inlet of the narrow segment. For a small value of *Re* (*Re* = 0.9), the axial velocity is found to rise moderately, and becomes constant (Fig. 14(a) and 15). Figures 14(b-d) and 15(a-b) show that a further increase in *Re* (*Re* = 14, 32, and 42), causes axial velocity to decrease along the narrow section of the channel. Figure 15(b) shows that the fluctuation of the longitudinal velocity gradient at the inlet of the narrow channel is caused by the a sudden decrease in pressure at the channel outlet. Figure 17 shows that the longitudinal velocity gradient corresponds to the null velocity gradient, which asserts the linearity of $(\frac{\partial U^*}{\partial x^*})_{\max}$. In the narrow section of the channel, longitudinal velocity is found to exist, which suggests a deviation of velocity profile from the Poiseuille flow.

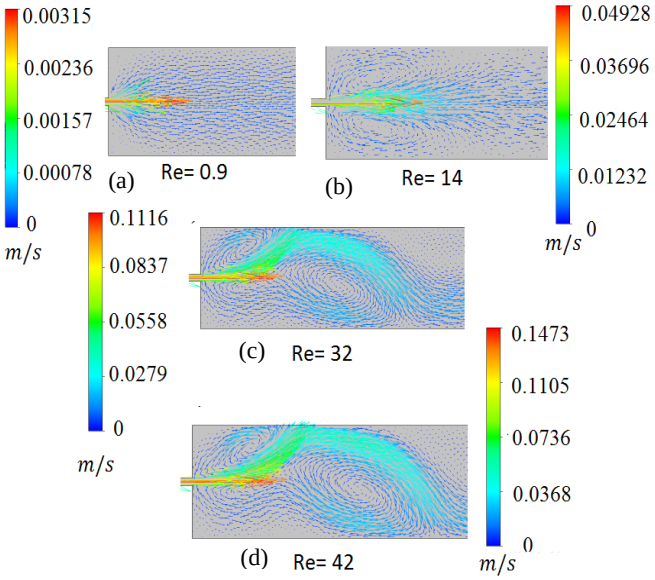

Fig. 14. Velocity vector fields for various *Re*.

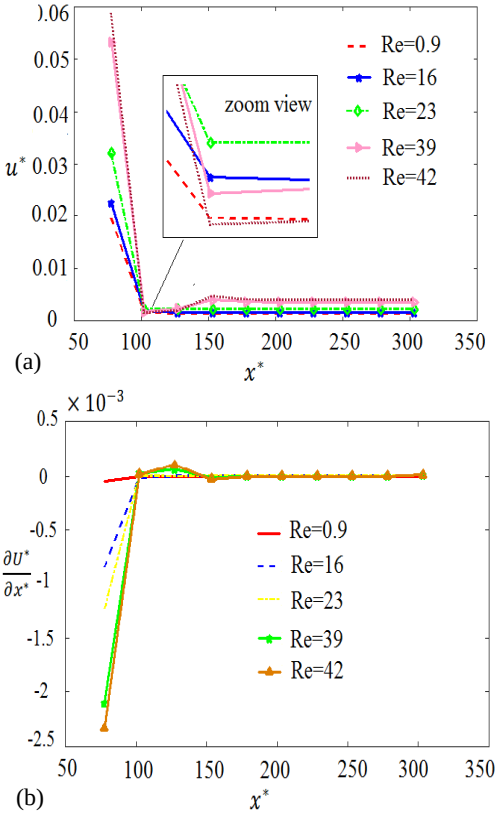

Fig. 15. Profiles of (a) U* & its gradient (b) $\frac{\partial U^*}{\partial x^*}$ at various *Re*.

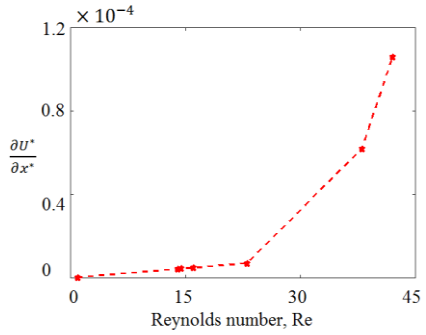

Fig. 16. Profile of longitudinal velocity gradient ($\frac{\partial u^*}{\partial x^*}$) max at various Re.

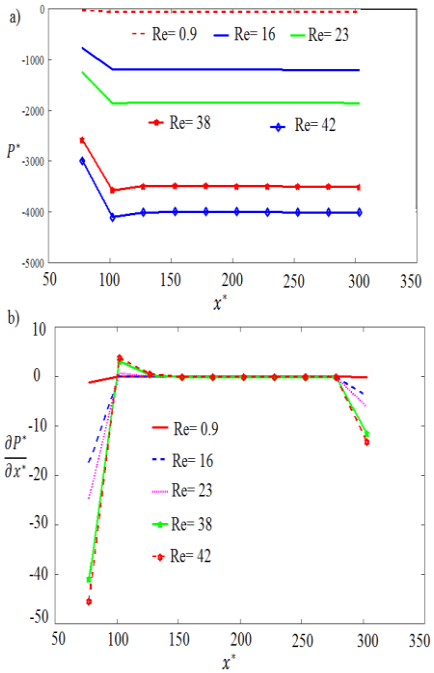

Fig. 17. Variations of (a) P* and its longitudinal gradient (b) $\frac{\partial P^*}{\partial x^*}$ with non-dimensional length x* at various *Re*.

4.5. Effect of Skin Friction and Pressure Coefficients

In this section, the effects of the pressure coefficient are defined by $C_p = 2(p_w - p_{in})/(\rho u_{in}^2)$ and the skin friction coefficient is defined by $C_f = 2\tau_w/(\rho u_{in}^2)$ (Kadja *et al.* 2002; Dhinakaran *et al.* 2013) on flow patterns along the lower and corner walls have been discussed and presented in the Fig. (18-19) at h = 15. Here, p_w, p_{in}, u_{in}, and $\tau_w = \mu\, \partial u/\partial y\,|_{y=0}$ denote the

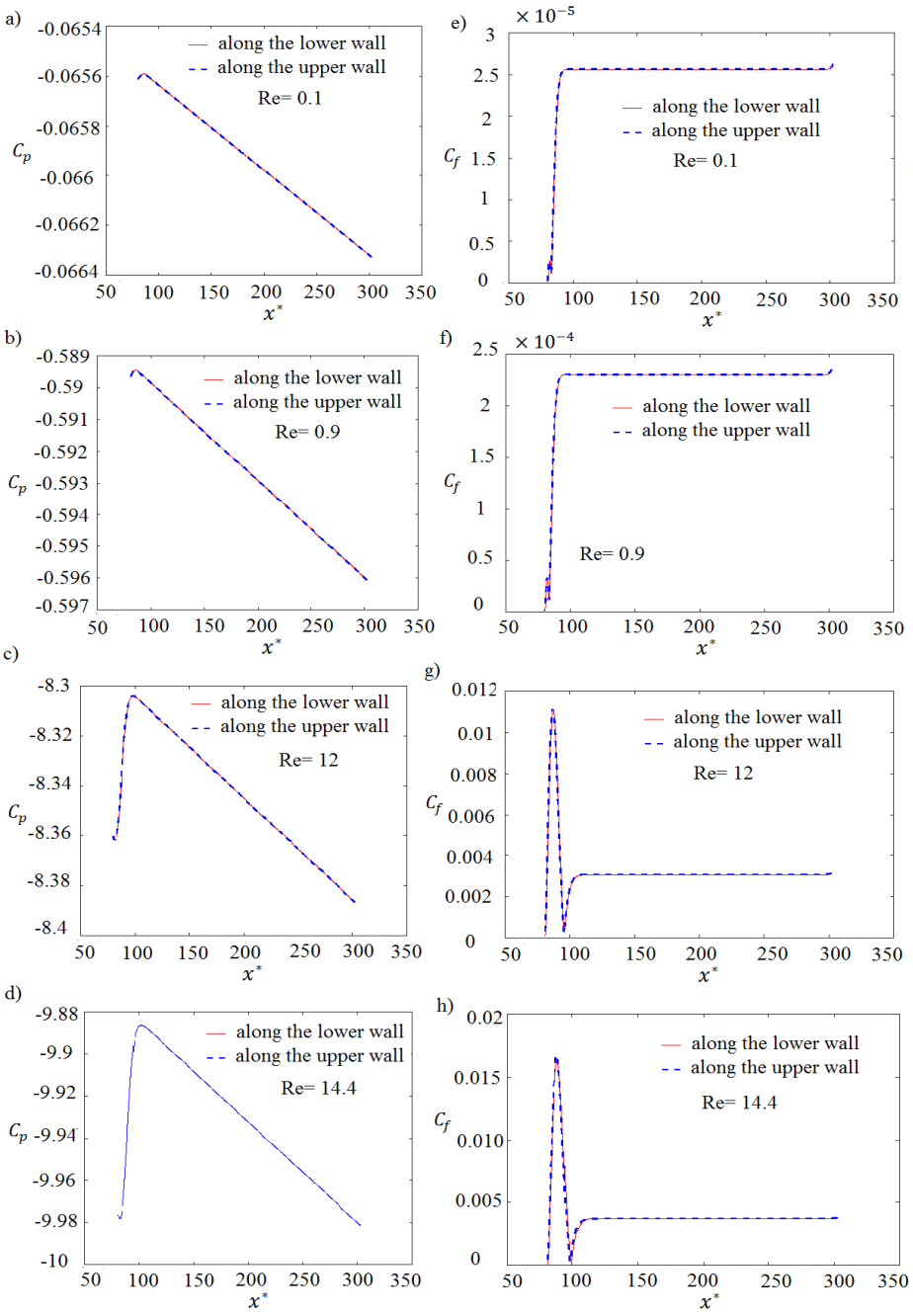

Fig. 18. Plots of (a-d) pressure and (e-h) friction coefficients for 0.1≤ Re ≤ 14.4.

wall pressure, inlet centerline pressure, inlet velocity, and the shear stress on the walls respectively (Dhinakaran *et al.* 2013). The detachment and reattachment points of flow along the corner walls (Fig. 18, 19), where it is also revealed that streamwise velocity changes sign as the sign of the parameter changes. From Fig. 19(a-h), we see that the C_p and C_f curves ensure that pressure and skin friction coefficients are equal at both walls. It is also shown in Fig. 19(a-h) that pressure fluctuates at the face of the outlet section as *Re* increases and after attaining an extreme value it starts to fall when the central core flow strikes the corner walls of the channel. The upper wall curves of C_p show the discontinuity at the reattachment point, and the lower wall curves of C_p indicate a rise in pressure monotonically. For the change in the flow patterns, the upper and lower curves of C_p show discontinuity at the reattachment points. It should be noted that discontinuity at the reattachment points is caused due to the increase in the recirculation zone vertically. Consequently, the jet exit ratio increases due to the increase in pressure. The Cp curves often show discontinuities when more than two (*Re* > 14.4) recirculation zones occur at the corner walls of the channel (Fig. 19(a-h)).

4.6. Pressure Drop

The Fig. (22-24) present the drop in pressure between the inlet and outlet sections of the channel,

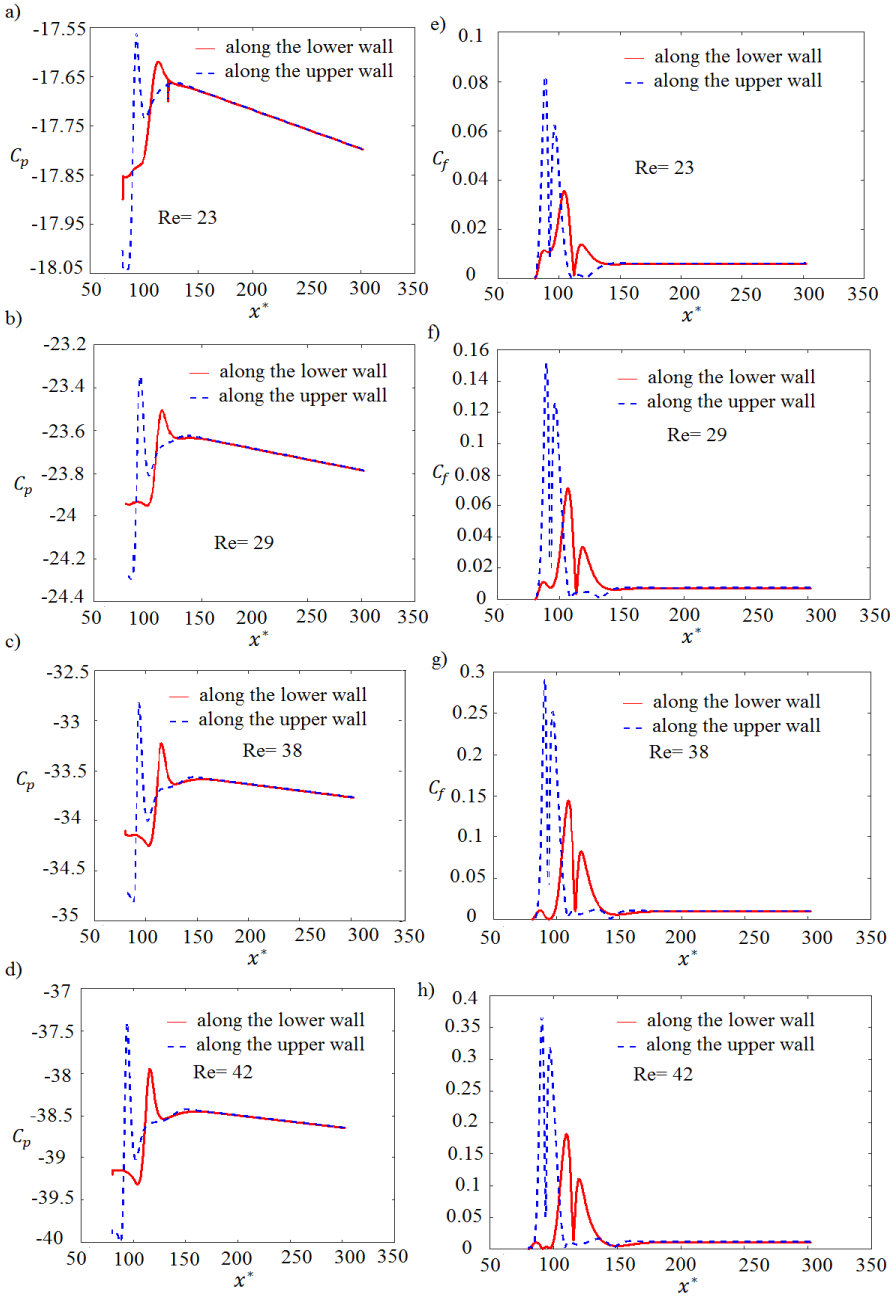

Fig. 19. Plots of (a-d) pressure and (e-h) friction coefficients for $23 \leq Re \leq 42$.

which shows pressure drop varies linearly with *Re*. It is found that pressure drop increases with the increase in *Re*. Transmission of blood occurs from the heart into the arteries in discrete pulses, i.e., throughout the body occurs due to blood pressure, for more details see. An increase in blood pressure through narrow arteries (which can be compared with the narrow section of the channel) results in the rupture of arteries and internal bleeding in the mitral valve (Alves *et al.* 2004). Tables 3a, 3b, and Tables 4a, 4b describe the blood pressure for various contraction ratios that depend on the distribution of *Re*. It is observed that blood pressure strictly depends on *h*. From Table (3-4) and Fig. (21-23), it is also found that blood pressure becomes normal at a small value of *Re* when the contraction ratio is high as expected. Furthermore, it is shown in Tables (3, 4) that there exists an inverse relationship between the contraction ratio and *Re*. To work with flow phenomena, it is very important to know the trend of the pressure recovery factor (p_{rf}), which reflects a sudden expansion effect on the downstream flow. It is observed that fluid static pressure increases when the fluid flows through a valve through the narrow section (vena contracta) to the valve's outlet section. Mathematically, p_{rf} is defined as $\sqrt{(p_2 - p_1)}$, where p_1, p_2 are the inlet and outlet pressures respectively.

The following two trends are observed in Fig. 23.

i) For a sufficiently large value of *Re*, the pressure recovery factor becomes higher.
ii) For each value of h, p_{rf} increases at the higher value of *Re*.

Table 3 (a-b) Blood pressure categories on the distribution of *Re* and h

a. normal pressure (< 120 mm=Hg)		b. pressure elevated [120 - 130] mm=Hg	
h	*Re*	h	*Re*
4	0.1 < *Re* ≤149.6	4	149.6 < *Re* ≤155.2
5	0.1 < *Re* ≤ 119.4	5	119.4 < Re ≤ 122
7.5	0:1 < *Re* ≤ 80.5	7.5	80.5 < *Re* ≤ 81.9
10	0.1 < *Re* ≤ 50.7	10	50.7 < *Re* ≤ 52.2
12	0.1 < *Re* ≤36.7	12	36.7 < *Re* ≤39.2
13.5	0.1 < *Re* ≤ 34.3	13.5	34.3 < *Re* ≤ 35.5
15	0.1 < *Re* ≤23.9	15	23.9 < *Re* ≤ 25.2

Table 4 (a-b) Blood pressure categories on the distribution of Re and h

a. hypertensive criteria [130 - 140] mm=Hg		b. high pressure [140-160] mm=Hg	
h	*Re*	h	*Re*
4	155.2 < Re ≤161.4	4	161.4 < *Re* ≤171.2
5	122 < Re ≤ 127.2	5	127.2< Re ≤ 138
7.5	81.9 < Re ≤ 83.5	7.5	83.5 < Re ≤ 91.9
10	49.2 < *Re* ≤ 50.7	10	50.7< *Re* ≤ 51.9
12	39.2 < *Re* ≤41.32	12	41.32< Re ≤ 47.5
13.5	35.5 < *Re* ≤ 39.9	13.5	39.9 < *Re* ≤ 42.2
15	25.2< *Re* ≤ 26.7	15	26.7< *Re* ≤ 31.9

In the considered geometry, many authors (Kang *et al.* 2006; Cantwell *et al.* 2010) investigated that the fluid flow through a narrow sections causes excess pressure drop (Δp_{exc}). Moreover, they stated that excess pressure drop is a common tool to know the effect of flow inertia. Here, an excess pressure drop is evaluated using the formula given by equation 7, and is accepted by many researchers (Kang *et al.* 2006; Castillo *et al.* 2014):

$$\Delta p_{exc} = \Delta p_{i0} - \Delta p_{in1} \times d_1 - \Delta p_{n1n_2} \times d_3 - \Delta p_{n2_0} \times d_2, \quad (7)$$

where Δp_{i0}, Δp_{in1}, and Δp_{n1n_2} are denoted as global pressure drop between inlet and outlet sections, inlet pressure at the entry of the narrow section, at the narrow section and at Δp_{n2_0} described as pressure drop in the outlet section respectively. It is seen that with the increase in *Re*, excess pressure drop increases at the onset for each contraction ratio (h= 4, 15) as shown in Fig. 24.

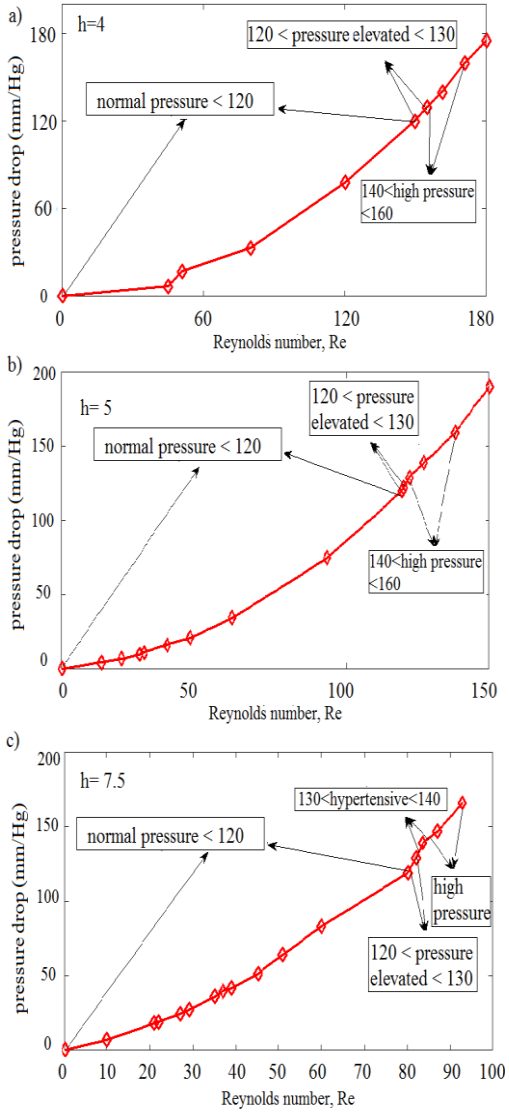

Fig. 20 (a-c): Plots of *Re* vs. pressure drop at various h = 4; 5 and 7.5.

5. CONCLUSION

In this study, numerical modeling of unsteady viscous laminar flow in a sudden contraction-expansion channel has been considered for various values of *Re* and compared the same with the flow of blood in the regurgitated mitral valve to anticipate cardiac arrest. The streamlines at various values of *Re*, and the bifurcation diagram presented in this work have a strong agreement with those of Patlazhan *et al.* (2017). Keeping the importance of the common problem of our life in mind, an attempt has been made to solve the above problem numerically. The method employed to solve the problem has been presented in section 4 and a detailed analysis of the numerical results of the problem considered here for variations in the values of various parameters associated with the model have been presented in the form of tables and graphs. The concluding remarks are as follows:

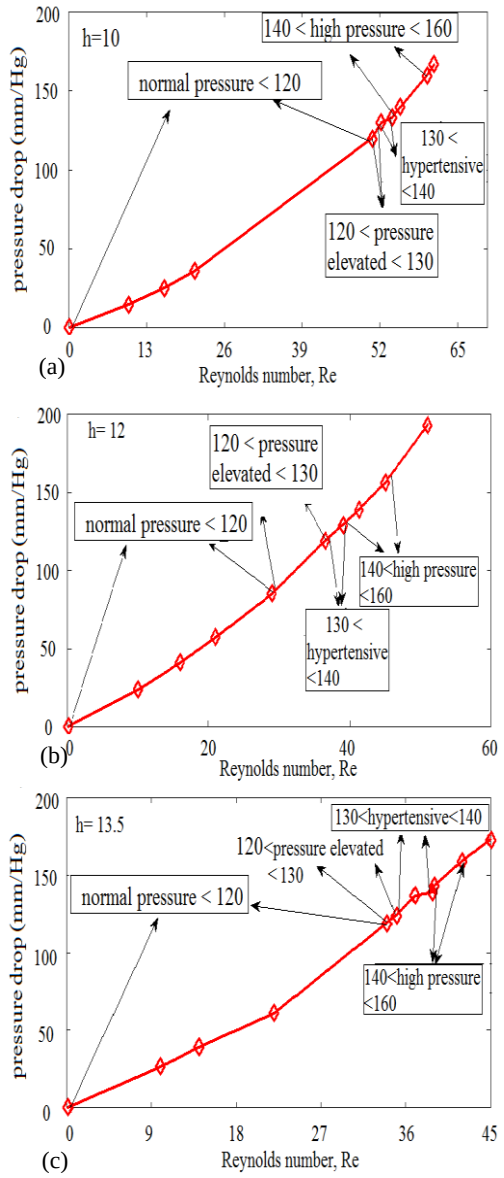

Fig. 21 (a-c): Plots of *Re* vs. pressure drop at various h = 10, 12 and 13.5.

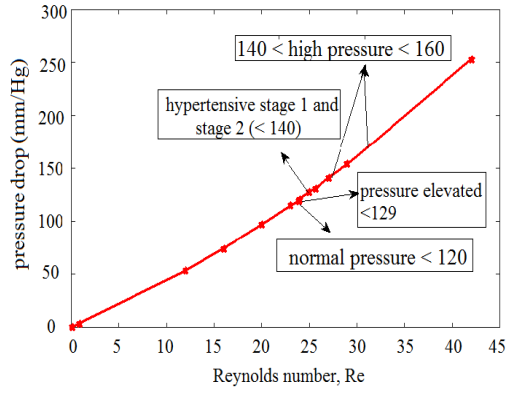

Fig. 22. Plot of *Re* vs. pressure drop at h = 15.

a. It is observed that an increase in *Re* increases the number of vortices, changes the flow symmetry for which recirculation becomes more complex, and decreases the rate of blood flow in the valve.

b. It is also observed that recirculation length increases as the channel depth increases. It has also been observed that an inverse relationship exists between Re_{cr} and h.

c. It is concluded that the value of the regression coefficient increases with the increase in h. It is also examined that blood pressure becomes normal at a small value of *Re*, when the contraction ratio is high as expected.

d. It is observed that fluid static pressure increases when the fluid flows through a valve from the narrow section (vena contracta) to the valve's outlet section. It is seen that with the increase in *Re*, the pressure recovery factor and excess pressure drop increases linearly at each contraction ratio.

In the end, we say that this work is analogous to the study of the flow of blood in the regurgitated mitral valve, and can be helpful to anticipate cardiac arrest. We have just attempted to show the way to solve a common problem in our real life through different numerical results. We hope that the results presented graphically in this paper would be helpful to the whole-mankind.

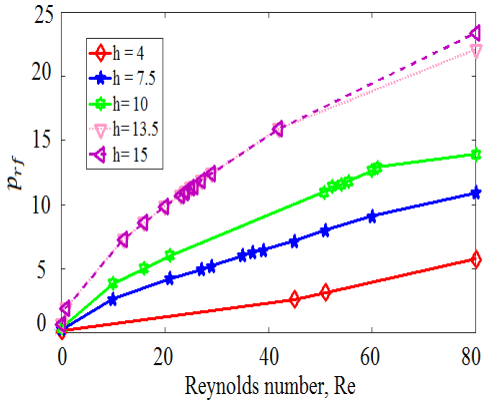

Fig. 23. Plot of *Re* vs. pressure recovery factor at various h.

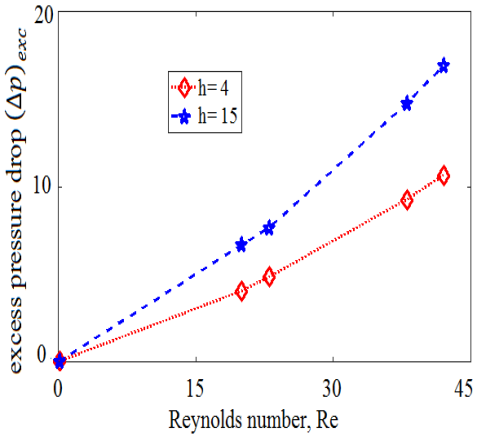

Fig. 24. Plots of Δp_{exc} vs. *Re*.

ACKNOWLEDGMENT

We are very grateful for all the reviewers' comments, which are become much more effective and helpful to improve the quality of the work.

REFERENCES

Abbot, D. E. and J. S. Kline (1962). Experimental investigation of subsonic turbulent flow over single and double backward facing steps. *Journal of Basic Engineering* 84, 317- 325.

Alves, M. A., J. P. Oliveira and T. F. Pinho (2004). On the effect of contraction ratio in visco elastic flow. *Journal* of *Non-Newtonian Fluid Mechanics* 122, 117-130.

Ashkezari, K. H. A., M. Dizani and A. Shamloo (2022). Integrating hydrodynamic and acoustic cell separation in a hybrid microfluidic device: a numerical analysis. *Acta Mechanica* 233(5), 1881-1894.

Astarita, G. and G. Greco (1968). Excess presssure drop in laminar flow through sudden contraction. *Industrial & Engineering Chemistry Fundamentals* 7(1), 27-31.

Bakirtas, I. and H. Demiray (2005). Weakly non-linear waves in a tapered elastic tube filled with an inviscid fluid. *International Journal* of *Non-Linear Mechanics* 40, 785-793.

Balloch, A., P. Townsend and M. F. Ebster (1995). On two and three-dimensional expansion flows. *Computers & Fluids* 24, 863-897.

Battaglia, F., J. S. Tavener, K. A. Kulkarni and L. C. A. Merkle (1997). Bifurcation of low reynolds number flows in symmetric channels. *American Institute of Aeronautics and Astronautics* 35, 99-105.

Boodaghi, M. and A. Shamloo (2020). A comparison of different geometrical elements to model fluid wicking in paper based microfluidic devices. *AIChE Journal* 66(1), e16756**.**

Boughamoura, A., H. Abbassi and B. Nasrallah (2003). Piston-driven laminar flow and heat transfer in a plane channel with a sudden expansion. *Computational Mechanics* 30, 410-420.

Cantwell, C. D., D. Barkley and M. H. Blackburn (2010). Transient growth analysis of flow through a sudden expansion in a circular pipe. *Physics of Fluids* 22(3), 1-15.

Castillo, T. L., O. G. Castrejn, J. F. J. Alvarado and O. Manero (2014). Prediction of excess pressure drop in contraction-expansion flow by molecular dynamics: Axi-symmetric and planar contaurations. *Journal of Non-Newtonian Fluid Mechanics* 210, 1-11.

Chen, J. H., G. W. Pritchard and J. S. W. Tavener (1995). Bifurcation for flow past a cylinder between parallel planes. *Journal of Fluid Mechanics* 284, 23-41.

Cherdron, W., F. Durst and J. H. Whitelaw (1978). Asymmetric flows and instabilities in symmetric ducts with sudden expansions. *Journal of Fluid Mechanics* 84, 13-31.

Davies, J., Z. Whinnett, D. Francis, K. Willson, R. Foale, I. Malik, A. Huges, K. Parker and J. Mayet (2006). Use of simultaneous pressure and velocity measurments to estimate arterial wave speed at a single site in humans. *American Journal of Physiology-Heart and Circulatory physiology* 290 (2), 15-35.

Dhinakaran, S., N. S. M. Oliveria, T. F. Pinho and A. M. Alves (2013). Steady flow of power-law fluids in a 1:3 planar sudden expansion. *Journal of Non-Newtonian Fluid Mechanics* 198, 48-58.

Drikakis, D. (1997). Bifurcation phenomena in incompressible sudden expansion flows. *Physics of Fluids* 9, 76-86.

Durst, F., F. C. J. Pereira and C. Tropea (1993). The plane symmetric sudden- expansion flow at low Reynolds numbers. *Journal of Fluid Mechanics* 248, 567- 581.

Fearn, R. M., T. Mullin and A. K. Cliffe (1990). Nonlinear flow phenomena in a symmetric sudden expansion. *Journal of* Fluid Mechanics 211, 595-608.

Formaggia, L., A. Quarteroni and A. Veneziani (2009). Cardiovascular and Mathematics. *Modeling and Numerical Simulation* 1, 15-27.

Ghosh, S., V. V. R. Kaushik, G. Das and K. P. Das (2012). CFD simulation of core annular flow through sudden contraction and expansion. *Journal of Petroleum Science and Engineering* 86-87, 153-164.

Hajji, H., L. Kolsi, K. Ghachem, C. Maatki, A. K. Hussein and M. N. Borjini (2021). Numerical study of heat transfer and flow structure over a microscale backstep. *Alexandria Engineering Journal* 60, 2759-2768.

Kadja, M., D. Touzopoulos and G. Bergeles (2002). Numerical investigation of bifurcation phenomena occurring in flows through planar sudden expansions. *Acta Mechanica* 153, 47-61.

Kang, K., W. K. Koelling and J. L. Lee (2006). Microdevice end pressure evaluations with Bagley correction. *Microfluid Nanofluid* 2, 223-235.

Korakianitis, T. and Y. Shi (2006). Numerical simulation of cardiovascular dynamics with healthy and diseased heart valves. *Journal of Biomechanics* 39, 1964-1982.

Leonard, P. B. (1979). A stable and accurate convective modeling procedure based on quadratic upstream interpolation. *Computer Methods in Applied Mechanics and Engineering* 19, 59-98.

Mishra, S. and K. Jayaraman (2002). Asymmetric flows in planar symmetric channels with large

expansion ratio. *International Journal for Numerical Methods in Fluids* 38(10), 945-962.

Moallemi, N, J. R. Brinkerhoff (2006). Numerical analysis of laminar and transitional flow in a planarsudden expansion. *Computers and Fluids* 140, 209-221.

Oliveira, M. S. N., L. E. Rodd, H. G. McKinley and L. Rodd (2008). Simulations of extensional flow in microrheometric devices. *Microfluidics and Nanofluidics* 5, 809-826.

Pal, R. and C. Hwang (1997). Flow of 2-phase Oil/Water through sudden expansion and contraction. *Chemical Engineering Journal* 68, 157-163.

Patlazhan, S. A., I. V. Kravchenko, R. Muller, Y. Hoarau, Y. Remond and A. Berlin (2017). Bifurcation of a Newtonian-fluid flow in a planar channel with sudden contraction and expansion. *Dokaldy Physics* 62, 145-148.

Saha, S. (2021a). Numerical simulation of turbulent flow through a sudden expansion channel: comparison between three model. *Lecture Notes in Mechanical Engineering* 49-56.

Saha, S. (2021b). A Survey on flow phenomena and heat transfer through expansion geometry. *Lecture Notes in Mechanical Engineering* 257-266.

Saha, S. and A. N. Das (2021). flow bifurcation phenomena of shear-thinning and newtonian fluids in a rectangular channel in presence of intermediate steps: using carreau-yasuda model. *Journal of Applied Fluid Mechanics* 14(4), 1283-1293.

Saha, S. and A. N. Das (2022). Hydro-thermal analysis of water-Al_2O_3 nanofluid flow through a sudden expansion channel with intermediate step. *Kuwait Journal of Science* 49(4).

Saha, S., P. Biswas and S. Nath (2020). Bifurcation phenomena for incompressible laminar flow in expansion channel to study Coanda effect**.** *Journal of Interdisciplinary Mathematics* 23(2), 493-502.

Saha, S., P. Biswas, K. Jha, A. N. Das and R. Choudhary (2021). Newtonian hydro-thermal phenomena through a sudden expansion channel with or without baffles. *Kuwait Journal of Science.*

Saha, S., S. Raut and A. N. Das (2022). Thermal enhancement and entropy generation of laminar water-Al2O3 nano-fluid flow through a sudden expansion channel with bell-shaped surface. *International Journal of Fluid Mechanics Research* 48(3), 65-78.

Sanmigue, R. E., C. Pino and C. M. Gutie. (2010). Global mode analysis of a pipe flow through a 1:2 axisymmetric sudden expansion. *Physics of Fluids* 22, 1-4.

Shamloo, A. and F. Y. Parast (2019). Simulation of blood particle separation in a trapezoidal microfluidic device by acoustic force. *IEEE Transactions on Electron Devices* 66(3), 1495-1503.

Shamloo, A., P. Vatankhah and M. A. Bijarchi (2016). Numerical optimization and inverse study of a microfluidic device for blood plasma separation. European *Journal of Mechanics-B/Fluids* 57, 31-39.

Shapira, M., D. Degani and D. Weihs (1990). Stability and existence of multiple solutions for viscous flow in suddenly enlarged channels. *Computers & Fluids* 18, 239-258.

Sobey, I. J. and G. P. Drazin (1986). Bifurcations of two-dimensional channel flows. *Journal of Fluid Mechanics* 171, 263-287.

Ternik, P. (2010). New contributions on laminar flow of inelastic non-Newtonian fluid in the two-dimensional symmetric expansion: Creeping and slowly moving flow conditions. *Journal of Non-Newtonian Fluid Mechanics* 165, 1400-1411.

Ternik, P., J. Marn and Z. Zunic (2006). Non-Newtonian fluid flow through a planar symmetric expansion: Shear-thickening fluids. *Journal of Non-Newtonian Fluid Mechanics* 13, 136-148.

Touzopoulos, D. and G. Bergeles (1998). Numerical investigations of the laminar steady incompressible sudden-expansion flow. *Proceedings European Congress on Computational Methods in Applied Sciences and Engineering* 98, 906-912.

Tsai, C. H., T. H. Chen, N. Y. Wang, C. H. Lin and M. L. Fu (2007). Capabilities and limitations of 2-dimensional and 3-dimensional numerical methods in modeling the fluid flow in sudden expansion microchannels. *Microfluid. Nanofluid* 3(1), 13-18.

Van Doormaal, J. P. and G. D. Raithby (1984). Enhancements of the SIMPLE method for predicting incompressible fluid flows. *Numerical Heat Transfer* 7, 147-163.

Verlinden, J. E., M. Madadelahi, E. Sarajlic, A. Shamloo, A. H. Engel, U. Staufer and M. K. Ghatkesar (2020). Volume and concentration dosing in picolitres using a two-channel microfluidic AFM cantilever. *Nanoscale* 12(18), 10292-10305.

Wang, J. J. and H. K. Parker (2004). Wave propagation in a model of the arterial circulation. *Journal* of *Biomechanical Engineering* 37, 457-470.

Zhao, W., K. T. Peter, R. Horswell, Y. Wang, W. Li, B. Heymsfield, W. Cefalu, H. Donna and H. Gang (2013). Aggressive Blood Pressure Control Increases Coronary Heart Disease Risk Among Diabetic Patients. *Diabetes Care* 36(10), 3287-3296.